JOURNAL OF APPLIED ELECTROCHEMISTRY **26** (1996) 1235–1244

Mass transport in a weakly stratified electrochemical cell

C. F. WALLGREN, F. H. BARK, R. ERIKSSON*, D. S. SIMONSSON*, J. PERSSON‡, R. I. KARLSSON‡

Department of Mechanics, Royal Institute of Technology, Stockholm, S 100 44 Sweden

Received 3 March 1995; revised 27 November 1995

A study of natural convection in an electrochemical system with a Rayleigh number of the order 10^{10} is presented. Theoretical and experimental results for the unsteady behaviour of the concentration and velocity fields during electrolysis of an aqueous solution of a metal salt are given. The cell geometry is a vertical slot and the reaction kinetics is governed by a Butler–Volmer law. To reduce the effects of stratification, the flush mounted electrodes are located (symmetrically) in the middle parts of the vertical walls. It is demonstrated, both theoretically and experimentally, that a weak stratification develops after a short time, regardless of cell geometry, even in the central part of the cell. This stratification has a strong effect on the velocity field, which rapidly attains boundary layer character. Measured profiles of concentration and vertical velocity at and above the cathode are in good agreement with numerical predictions. For a constant cell voltage, numerical computations show that between the initial transient and the time when stronger stratification reaches the electrode area, the distribution of electric current is approximately steady.

List of symbols

a_i	left hand side of equation system
b_i	right hand side of equation system
c'	concentration ($\mathrm{mol\,m^{-3}}$)
c	dimensionless concentration
c'_i	concentration of species 'i' ($\mathrm{mol\,m^{-3}}$)
c'_0	initial cell concentration ($300\,\mathrm{mol\,m^{-3}}$)
c_0	dimensionless initial cell concentration
c'_{wall}	concentration at electrode surface ($\mathrm{mol\,m^{-3}}$)
$\mathrm{d}\bar{x}$	increment solution vector in Newton's method
D_i	diffusion coefficient of species i ($\mathrm{m^2\,s^{-1}}$)
D_1	$0.38 \times 10^{-9}\ \mathrm{m^2\,s^{-1}}$
D_2	$0.82 \times 10^{-9}\ \mathrm{m^2\,s^{-1}}$
D	effective diffusion coefficient of the electrolyte ($0.52 \times 10^{-9}\ \mathrm{m^2\,s^{-1}}$)
$\bar{e}_x$	unit vector in the vertical direction
$\bar{e}_y$	unit vector in the horizontal direction
F	Faraday's constant ($96\,487\,\mathrm{A\,s\,mol^{-1}}$)
g	acceleration of gravity ($9.81\,\mathrm{m\,s^{-2}}$)
i	dummy referring to positive ($i = 1$) or negative ($i = 2$) ion
$\bar{i}'$	current density ($\mathrm{A\,m^{-2}}$)
$\bar{i}$	dimensionless current density
i'_0	exchange current density ($0.01\,\mathrm{A\,m^{-2}}$)
J_{ij}	Jacobian of system matrix
L	length of electrode (0.03 m)
$\bar{N}'_i$	transport flux density of ion i ($\mathrm{mol\,m^{-2}\,s^{-1}}$)
$\bar{n}$	unit normal vector
p'	pressure ($\mathrm{N\,m^{-2}}$)
p	dimensionless pressure
R	gas constant molar ($8.31\,\mathrm{J\,K^{-1}\,mol^{-1}}$)
R_i	residual of equation system
Ra	Rayleigh number $g\beta L^3 c_0/\nu D$ (2.54×10^{10})
Sc	Schmidt number ν/D (1730)
t'	time (s)
t	dimensionless time
T	temperature (293 K)
$\bar{u}'$	velocity vector ($\mathrm{m\,s^{-1}}$)
$\bar{u}$	dimensionless velocity vector
U	characteristic velocity in the vertical direction
$V_{\pm}$	potential of anode and cathode, respectively
x'	spatial coordinate in vertical direction (m)
x	dimensionless spatial coordinate in vertical direction
$\bar{x}$	solution vector for c, Φ and $\bar{u}$
y'	spatial coordinate in horizontal direction (m)
y	dimensionless spatial coordinate in horizontal direction
z_i	charge number of ion i

Greek symbols

α	symmetry factor of the electrode kinetics, 0.5
β	volume expansion coefficient ($1.24 \times 10^{-4}\,\mathrm{m^3\,mol^{-1}}$)
η_s	surface overpotential
Γ	constant in equation for the electric potential (−5.46)
δ_s	diffusion layer thickness
δ	scale of diffusion layer thickness
κ	constant relating $\partial c/\partial y$ to the Butler–Volmer law (0.00733)
ν	kinematic viscosity ($0.9 \times 10^{-6}\,\mathrm{m^2\,s^{-1}}$)

* Department of Applied electrochemistry.
‡Vattenfall Utveckling AB, Alvkarleby.

0021-891X © 1996 Chapman & Hall

Greek symbols

ρ density ($g\,m^{-3}$)
Φ' electric potential of electrolyte ($V\,m^{-1}$)
Φ dimensional electric potential of electrolyte
∇' $(\partial/\partial x', \partial/\partial y')$ (m^{-1})
∇ $(\partial/\partial x, \partial/\partial y)$

1. Introduction

Natural convection appears frequently in electrochemical systems such as cells for metal refining and lead acid batteries. In cases with vertically oriented electrodes, the strength of the convective motion is often measured in terms of the Rayleigh number (Ra). This nondimensional number is proportional to L^3, where L is the linear dimension of the electrodes*, and to the scale of the change of concentration due to the electrode reactions. At high Rayleigh numbers, which appear also in small systems with moderate changes in concentration, the mass transfer is dominated by convection. The importance of convective mass transfer is even more pronounced for large systems, for example, in metal refining or large batteries for load levelling. A good physical understanding of the motion of the liquid electrolyte is thus essential for improving the efficiency of operation of a variety of systems.

In closed electrochemical systems, or in systems with a weak throughflow, natural convection is strongly influenced by stratification of the electrolyte. These effects are usually undesirable. For example, in electroplating, stratification is tantamount to an inhomogeneous resistivity, which leads to a locally increased current density in regions of higher concentration. As a result, the thickness of the plated metal layer will be nonhomogeneous. By vigorous stirring or by a strong forced convective motion, effects of stratification may be removed.

The paper by Wagner [1], in which effects of steady natural convection on the limiting current density on a copper cathode in a nonstratified aqueous solution of copper sulfate was investigated, was pioneering in making use of basic principles of fluid mechanics to quantify the importance of electrolyte motion in an electrochemical cell. The procedure used by Wagner [1], which relied on the momentum integral method for determining the natural convection, was further elaborated upon by Awakura *et al.* [2]. Comparisons with experiments were made by Awakura *et al.* [3], who, among other things, investigated how different initial concentrations affected the steady velocity distribution on the cathode. Transient effects on short time scales, compared to the time scale for evolution of the system toward its steady state, have been studied theoretically and experimentally by Fukunaka and Kondo [4] and Fukunaka *et al.* [5]. In none of these studies were effects of stratification accounted for. So far, for large cells, such effects appear to have only been dealt with by using crude semiempirical methods. A summary of the state of the art has been given by Fukunaka and Kondo [6].

In contrast to the case of large cells, and cells of intermediate size as that considered in the present work, stratification in small cells has recently been investigated in some detail and is reasonably well understood. A recent review of the role of convective mass transport in small cells has been given by Bark and Alavyoon [7]. One of the main differences between the behaviour of small cells and large ones is that, in the former case, very strong effects of stratification are felt very quickly after a short initial transient whereas in the latter case, a longer buildup time is needed before the motion is completely dominated by stratification.† However, as will be demonstrated in the present work, the time required for effects of stratification to be felt in a system of intermediate size is shorter than expected. The implications of this result for large cells will be investigated in future work.

Some comments on related work in the heat transfer literature are in order. Approximate analytical studies of steady natural convection of high Prandtl number fluids in enclosures have been carried out by Gill [8] and Kimura and Bejan [9]. In both these investigations the horizontal walls were insulated, but the thermal forcing at the vertical walls were different. In the paper by Gill [8], the vertical walls were assumed to be kept at fixed different temperatures whereas in the paper by Kimura and Bejan [9], constant fluxes of heat were prescribed. The exact solution given by Gill for the special case of linear stratification is in fact, when applied to the whole cell height, equal to that given by Kimura and Bejan. In Gill's approximate analytical solution for nonlinear stratification, the interrelation between the stratification and the steady state horizontal motion in the interior is demonstrated. The solution also shows that for strong stratification, the dual structure of the boundary layer vanishes. For the case considered by Kimura and Bejan [9], on the other hand, the boundary layers are of constant thickness and the interior is completely stagnant.

For certain classes of core stratifications and boundary conditions, similarity solutions for the steady boundary layer flow along a vertical wall can be found. Several solutions are given by Gebhart *et al.* [10]. A broader class of steady similarity solutions has been given by Semenov [11]. These solutions are investigated by Henkes and Hoogendoorn [12]. The backflow occurring in the outer part of the boundary layer in a stably stratified environment leads to loss of parabolicity for the mathematical problem, and

* In the present work, the bulk concentration of the electrolyte is chosen as the concentration scale. One may alternatively take the current density on the electrodes as a measure of the forcing of the motion. In that case, one obtains that $Ra \sim L^4$.

† The most important difference between these cases is, as is well known, that the motion of the electrolyte in large cells is turbulent but laminar in small cells.

Henkes and Hoogendoorn conclude that for some forms of stratification, similarity solutions cannot be applied as boundary conditions for the complete numerical problem. A rough approximate procedure, called the 'modified local similarity method', has been proposed by Webb [13]. Similarity methods may, in certain cases, also be used for unsteady heat transfer problems in enclosures. A recent example is the work by Worster and Leitch [14].

The transient behaviour of vertical boundary layers in a nonstratified environment has been considered in detail by Carey [15, 16] by using a combination of singular perturbation techniques for large values of the Prandtl number and numerical analysis. In these studies, the boundary layer response to an instantaneously increased wall temperature or wall heat flux was computed. The dual structure of the boundary layer was shown to prevail during the whole transient, and the presence of an overshoot for both temperature and velocity before the steady state is reached was clearly demonstrated. The results given by Carey, although being informative for the case studied in the present work, do not account for the interaction between the two vertical boundary layers which exists in the present problem. This interaction, which was discussed in some detail by Gill [8], takes place via local entrainment into one of the boundary layers and detrainment out from the other. During the early stages of the electrolysis considered in the present paper, this kind of interaction between the vertical walls is of importance.

A recent review of transient heat transfer in enclosures with prescribed temperature differences of the vertical walls has been given by Hyun [17]. The roles of three distinct processes occurring on different time scales during heat up of an enclosed fluid are emphasized: the establishment of boundary layers, convective redistribution of heat and finally diffusive smoothing. The time scales for these processes can be expressed in terms of the Brunt–Väisälä frequency and the Prandtl and Rayleigh numbers. An analysis along these lines is not attempted in the present work, which is a first step into an essentially unexplored area. In a recent numerical study by Poujol *et al.* [18] of transient natural convection in an enclosure at high Prandtl and Rayleigh numbers, boundary conditions at the vertical walls that partially resemble those in the present work are investigated. The evolution of the temperature field in the top and bottom regions of the enclosure shows qualitative agreement with that of the concentration field considered here.

The present work reports on theoretical and experimental investigations of the system |Cu(s)|$CuSO_4$ (aq)|Cu(s)| in a case with weak stratification. The considered value of Ra is large but, for simplicity, chosen such that laminar flow prevails. The results obtained are thus not directly applicable to the large cells used in industry for copper refining, in which the electrolyte is strongly turbulent. However, the parameter range investigated may be seen as an intermediate case between the above application and the small cells studied in some detail, both theoretically and experimentally, by Karlsson *et al.* [19], Eklund *et al.* [20] and Bark *et al.* [21]. As it will be seen in the following Sections, several of the phenomena found, some of which were unexpected in the present intermediate case, will most likely appear also in a full scale cell for refining of copper but then interacting with a complicated turbulent flow.

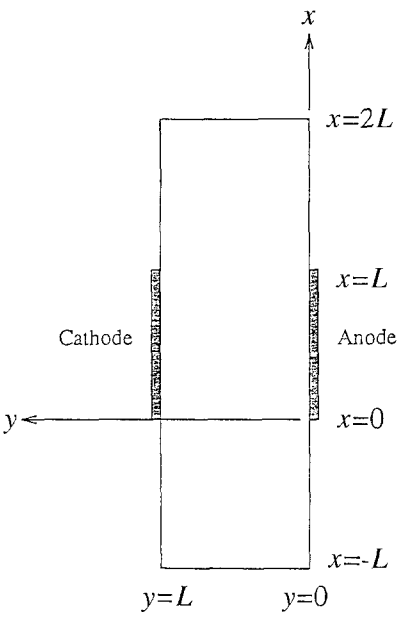

Fig. 1. Geometry of the cell.

2. Formulation of numerical problem

The geometry of the two-dimensional cell is shown in Fig. 1. The vertical walls are divided into three sections, each of length L, where the middle sections consist of the flush mounted electrodes. The distance between the electrodes is also set equal to L. The analysis applies to a binary electrolyte, and when numerical values are assigned to physical constants, they correspond to a copper refining cell without supporting electrolyte.

The electrochemical reactions at the electrodes are

$$\begin{aligned} &\mathrm{Me} \longrightarrow \mathrm{Me}^{z_1} + z_1 \mathrm{e}^- \qquad \text{anode} \\ &\mathrm{Me}^{z_1} + z_1 \mathrm{e}^- \longrightarrow \mathrm{Me} \qquad \text{cathode} \end{aligned} \tag{1}$$

where z_1 is the charge number of the metal ion Me^{z_1}. The mass flux vector of species i in the electrolyte, where $i = 1, 2$, is given by the Planck–Nernst law:

$$\bar{N}_i' = -\frac{FD_i}{RT} c_i' z_i \nabla' \Phi' - D_i \nabla' c_i' + c_i' \bar{u}' \tag{2}$$

Mass conservation of each species is ensured by the following equations

$$\frac{\partial c_i'}{\partial t'} = -\nabla' \cdot \bar{N}_i' \tag{3}$$

and the electric current density is quantified by Faraday's law,

$$\bar{i}' = F(z_1 \bar{N}_1' + z_2 \bar{N}_2') \tag{4}$$

The electrolyte considered in the present work (i.e.,

$CuSO_4$(aq)) can, as an accurate approximation, be considered as electrically neutral. In what follows, the ions Cu^{2+} and SO_4^{2-} are labelled species 1 and 2, respectively. Thus

$$z_1 c_1' + z_2 c_2' = 0 \tag{5}$$

which implies a nondivergent electric current, that is,

$$\nabla' \cdot \bar{i}' = 0 \tag{6}$$

It is convenient to introduce a new variable for the concentration, $c' = z_1 c_1' = -z_2 c_2'$. If Equation 2 is put into Equation 3 and the result is multiplied by z_i, the two equations (one for each 'i') can be combined to give

$$\frac{\partial c'}{\partial t'} + \bar{u}' \cdot \nabla' c' = D \nabla'^2 c' \tag{7}$$

where $D = 2D_1 D_2/(D_1 + D_2)$. An equation for the electric potential, Φ', is derived from Equations 2, 4 and 6 as

$$\frac{F}{RT} \Gamma \nabla' \cdot (c' \nabla' \Phi') + \nabla'^2 c' = 0 \tag{8}$$

where $\Gamma = 2(D_1 + D_2)/(D_1 - D_2)$.

For the electrochemical part of the problem (i.e., the determination of c' and Φ') two boundary conditions are needed. The prescribed electric potentials of the electrodes are V_+' (anode) and V_-' (cathode). One boundary condition is provided by the Butler–Volmer law, which is taken to be of the form

$$\bar{i}'(x') \cdot \bar{e}_y = i_0' \left[\exp\left(\alpha \frac{F}{RT} \eta_s \right) - \frac{c_{\text{wall}}'(x')}{c_0'} \exp\left(-(1-\alpha) \frac{F}{RT} \eta_s \right) \right] \tag{9}$$

where η_s is the surface overpotential and the constant i_0' is the exchange current density. The normal component of the current density, $\bar{i}'(x') \cdot \bar{e}_y$, is defined as positive when the current leaves the electrode and enters the electrolyte. Condition 9 is thus applicable to both electrodes. An additional boundary condition is obtained by the fact that only the positive cupric ions carry charge across the electrode surfaces, that is,

$$\bar{N}_1' \cdot \bar{e}_y = \frac{\bar{i}' \cdot \bar{e}_y}{z_1 F}$$

$$\bar{N}_2' \cdot \bar{e}_y = 0 \tag{10}$$

Boundary conditions 9 and 10 can, when combined with Equations 2 and 4, be formulated as boundary conditions for c' and Φ', which will later be presented in nondimensional form. At all insulated boundaries, the gradients of c' and Φ' perpendicularly to the boundary are set to zero.

The governing equations for the three remaining variables, i.e. the velocity field $\bar{u}' = (u', v')$ and the pressure field p', are the two-dimensional Navier–Stokes equations for incompressible flow and the continuity equation:

$$\frac{\partial \bar{u}'}{\partial t'} + \bar{u}' \cdot \nabla' \bar{u}' = -\frac{1}{\rho} \nabla' p' + \nu \nabla'^2 \bar{u}' - g\beta(c' - c_0') \bar{e}_{x'} \tag{11}$$

$$\nabla' \cdot \bar{u}' = 0 \tag{12}$$

The Boussinesq approximation has been used in Equation 11. Boundary conditions for u' and v' are the no-slip conditions. Before the equations are written in nondimensional form, an estimate, U, of the velocity scale in the vertical direction has to be found. Taking the length scale in the vertical direction to be L and that in the horizontal direction to be δ, scale analysis of Equation 7 with $\partial c'/\partial t' = 0$ gives $U \sim DL/\delta^2$. Comparing the different terms in the Navier–Stokes equation in the vertical direction, and assuming that inside the concentration boundary layers there is a balance between buoyancy and viscous forces, it is concluded that $\delta \sim LRa^{-1/4}$, which gives $U \sim DRa^{1/2}/L$. The Rayleigh number is defined as $Ra = g\beta c_0' L^3/D\nu$. A more extensive scale analysis arriving at the same result is given by Bejan [22].

The following nondimensional variables are now introduced:

$$y = \frac{y'}{L}, \quad x = \frac{x'}{L}, \quad (V_+, V_-, \Phi) = \frac{F}{RT}(V_+', V_-', \Phi')$$

$$c = \frac{c'}{c_0'} - 1, \quad \bar{u} = \frac{\bar{u}'}{U}, \quad t = \frac{Ut'}{L}, \quad p = \frac{p'}{\rho U^2},$$

$$\bar{i} = \frac{\bar{i}' L}{2D_1 F c_0'}$$

Substitution of the physical variables in terms of their nondimensional counterparts gives, with the expression for U deduced above, a system of nondimensional equations for $c, \Phi, \bar{u}$ and p.

$$\frac{\partial c}{\partial t} + \bar{u} \cdot \nabla c = Ra^{-1/2} \nabla^2 c$$

$$\Gamma \nabla \cdot [(1+c) \nabla \Phi] + \nabla^2 c = 0$$

$$\frac{\partial \bar{u}}{\partial t} + \bar{u} \cdot \nabla \bar{u} = -\nabla p + Sc(Ra^{-1/2} \nabla^2 \bar{u} - c\bar{e}_x)$$

$$\nabla \cdot \bar{u} = 0 \tag{13}$$

where the Schmidt number $Sc = \nu/D$.

The nondimensional boundary conditions become

$$\frac{\partial c}{\partial y} = \pm\kappa[\exp(\alpha\eta_s) - (1 + c_{\text{wall}}) \exp(-(1-\alpha)\eta_s)] \qquad 0 \le x \le 1$$

$$\bar{n} \cdot \nabla c = 0 \qquad x < 0 \text{ or } 1 < x$$

$$\frac{\partial \Phi}{\partial y} = \frac{1}{2(1+c)} \frac{\partial c}{\partial y} \qquad 0 \le x \le 1$$

$$\bar{n} \cdot \nabla \Phi = 0 \qquad x < 0 \text{ or } 1 < x$$

$$\bar{u} = 0 \tag{14}$$

where $\kappa = Li_0'/2D_1 F c_0'$ and the unit vector $\bar{n}$ is perpendicular to the respective boundary. The following

parameter values were used in the calculations:

$$Ra = 2.54 \times 10^{10}$$

$$Sc = 1730$$

$$\Gamma = -5.46$$

$$\kappa = 7.33 \times 10^{-3}$$

The numerical values of the physical parameters are given in the list of notations. Wide ranges of values for certain parameters can be found in the electrochemical literature (e.g., see [23–25]), and the values for the exchange current density, i_0', and diffusivities, $D_{1,2}$, have been chosen within these ranges.

2.1. *Numerical method*

The system of equations for c, ϕ, u and v are discretized using a Crank–Nicolson finite volume method [26], and a pressure correction scheme [27] was applied to solve for p using the continuity equation‡. The first set of equations was solved implicitly at every timestep with Newton's method. In terms of the left and right hand sides of the system of equations, a_i and b_i, respectively, each Newton iteration can be written:

$$J_{ij}\,\mathrm{d}x_j = -R_i \tag{15}$$

where $J_{ij} = \partial a_i(\bar{x}^k)/\partial x_j$, $R_i = b_i(\bar{x}^n) - a_i(\bar{x}^k)$. $\bar{x}^k$ is the solution from the previous iteration and $\bar{x}^n$ is the solution from the previous timestep. The linearized equations were solved by the GMRES-algorithm [28] with incomplete LU-factorization and the Jacobian calculated analytically, and updated as $\bar{x}^{k+1} = \bar{x}^k + \mathrm{d}\bar{x}$. The vector $\bar{x}$ is here the solution vector for c, Φ, u and v. When

$$\sum_{i=1}^{m} \frac{b_i - a_i(\bar{x}^k)}{a_i(\bar{x}^k)} < 10^{-3}$$

where m is the number of unknowns, the pressure correction scheme is applied using the 'conjugate gradient method' [29]. After updating the pressure and velocity fields once more, the next timestep is taken with $t^{n+1} = t^n + \mathrm{d}t$ and $\bar{b} = \bar{b}(\bar{x}^{n+1})$.

The discretizations were made on a nonuniform and staggered grid, and the discretized equations are second order accurate both in time and space. A mesh with 100×135 gridpoints has been used, where the smallest grid spacing in the horizontal direction was located at the vertical walls and equal to 1.0×10^{-3}. This spacing was necessary to resolve the concentration boundary layers which were only about 0.01 units thick. Tests were also run with a reduced number of gridpoints (67×50), and since the result was only marginally affected by this change it was concluded that the use of the higher number of points well captured the physical behaviour of the flow. Because of the explicit nature of the pressure correction scheme, the timestep was limited to about 10^{-3} to obtain accurate results.

‡ When using this method, one has to specify the mathematically artificial boundary condition $\bar{n} \cdot \nabla p = 0$ on solid walls.

2.2. *Experimental methodology*

The length L in the experimental cell was 0.03 m, while the thickness (i.e., the distance between the nonelectrode vertical side walls) was only 0.01 m to minimize errors in the concentration measurements. The electrodes were made of pure copper (SS 5010: > 99.9%) and covered the whole cell width, giving an active area of $3 \times 10^{-4}\,\mathrm{m}^2$ each. They were connected to a voltage source, which was set to the desired value. The electrolyte was an 0.3 molar aqueous solution of $CuSO_4$, and the mean current density ($46\,\mathrm{A\,m^{-2}}$) gave average concentration changes across the boundary layers of around 20% of the bulk concentration, with a maximum value below 30%. The applied current was thus well below the limiting current. Before each experiment the electrode surfaces were polished with emery paper (grade 600) until no visible inhomogeneities could be found.

The velocity measurements were performed by laser–Doppler velocimetry at Vattenfall Utveckling AB in Älvkarleby. A TSI fibre-optic system with a 0.122 m focal distance transmitting lens fitted to the fibre probe was used. The laser beams had a wavelength of 488 mm which gave an ellipsoidal measuring volume with a diameter of 0.036 mm and a length of 0.26 mm. The output effect was about 10^{-2} W, and one of the beams was frequency shifted in order to determine the sign of the velocity. Silicon carbide particles with a mean diameter and density of 1.5 μm and $3200\,\mathrm{kg\,m^{-3}}$, respectively, were added to the electrolyte for light-reflecting purposes. The velocity at each position was measured for 10 s with a mean data rate of 30 Hz, and a TSI IFA750 signal processor analysed the Doppler bursts. Standard TSI software (FIND) was used for the statistical evaluation. The probe was mounted on a table adjustable by micrometer screws, and the time needed to move the probe from one position to the next was approximately 5 s, giving a total scanning time of a full velocity profile with 25 measuring points of about 6 min. Because the steep density gradients close to the electrodes, deflected the laser light, it was necessary to use an angle between the beams and the electrode surface of approximately 5° in order to focus on the electrode surface [19]. Despite this angle, the extension of the measuring volume made it difficult to accurately determine the position of the surface.

The probe beam deflection method, described by Eriksson [30], was used to measure concentration gradients at the vertical walls.

3. Results and conclusions

Figures 2 to 5 show the development of the velocity and concentration fields as plotted streamlines and iso-concentration lines at different times. In Fig. 2(a), showing the concentration field after twenty seconds, the gradients are limited to thin boundary layers which have begun to propagate in the vertical directions due to buoyancy forces. The thickness of

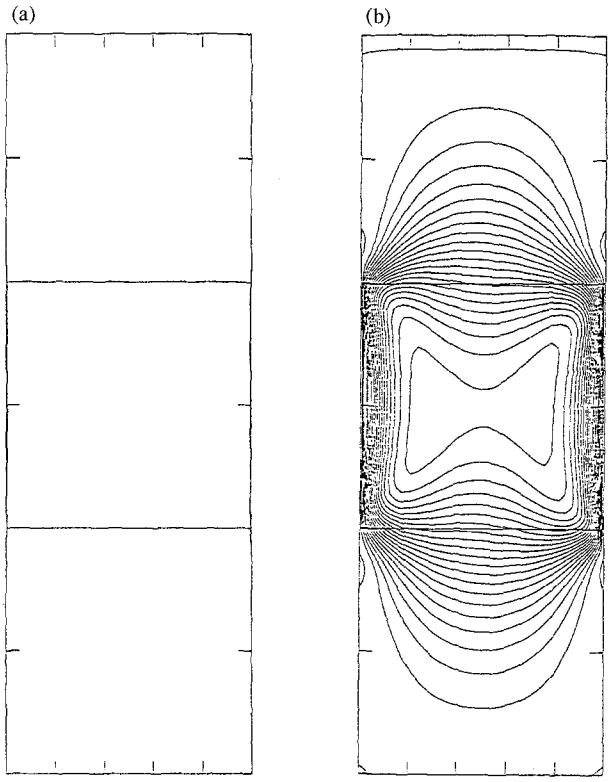

Fig. 2. Computed concentration (a) and velocity (b) fields for $t = 20$ s. $\Delta c = 0.01$ and $\Delta\psi = 2e^{-4}$.

these boundary layers is denoted as δ_S. For small times $\delta_S \sim \delta$. For large times, $\delta_S \ll \delta$. The velocity field shown in Fig. 2(b) increases steeply from the wall out to its maximum value at $y \sim \delta_S$ and decays more slowly outside δ_S where $c \approx c_0$. Comparing this situation with that of natural convection in a nonstratified semiinfinite fluid at the same Rayleigh and Schmidt numbers, it is found that the viscous layer at the trailing edges in the latter case has spread to a thickness of the same order as the cell width. This is in agreement with the velocity field in Fig. 2(b), and demonstrates that stratification does not yet influence the flow field between the electrodes. However, Fig. 2(b) also shows that the vertical walls considerably affect the horizontal motion in the cell, where strongly entraining and detraining boundary layers create a central vortex which redistributes variations in concentration between the boundary layers and the core region, thus initiating the early development of stratification between the electrodes. This is described by Gill [8] as a competition for fluid between the boundary layers.

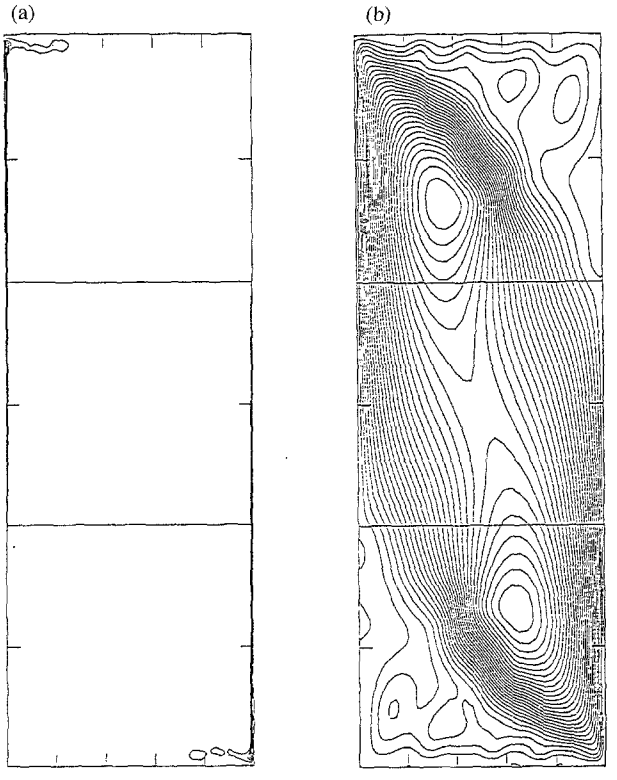

Fig. 3. Computed concentration (a) and velocity (b) fields for $t = 2$ min. $\Delta c = 0.01$ and $\Delta\psi = 2e^{-3}$.

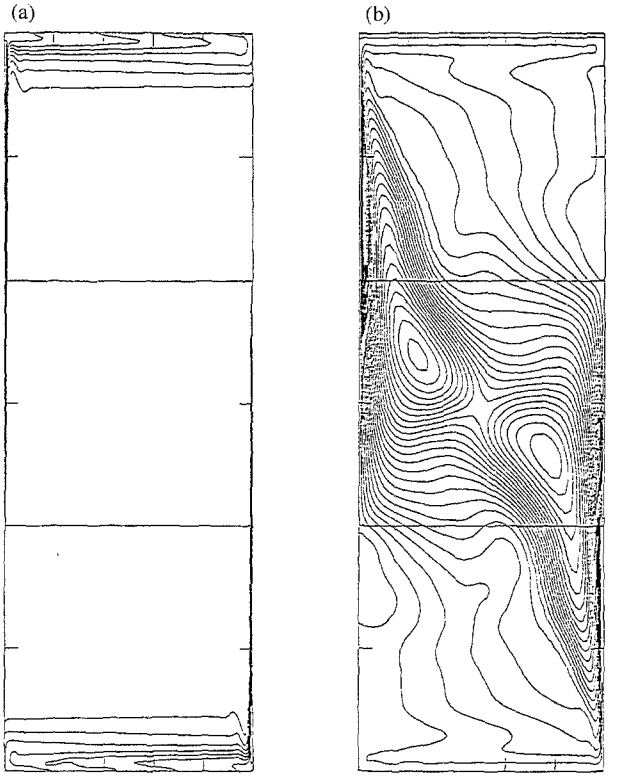

Fig. 4. Computed concentration (a) and velocity (b) fields for $t = 12$ min. $\Delta c = 0.01$ and $\Delta\psi = e^{-3}$.

Figures 3(a) and (b) show the situation after 2 min when the concentration boundary layers have just reached the top and bottom of the cell. Large pressure gradients have developed in these areas to retard the flow, and the streamlines show that the flow goes through a sharp change of direction at the cell corners. This development continues in Figs 4 and 5, which show the stratification moving into the interior from the horizontal boundaries. Realizing now that the development in the upper half is qualitatively the same as that in the lower half, only with different signs for the concentration and velocities, we choose to study only the latter in the following. When stratification begins to develop at the bottom of the cell, fluid elements around $y = \delta_S$ are dragged down into the stratified area by heavier fluid closer to the wall. Since this course of events is faster than the diffusion process that eventually evens out concentration

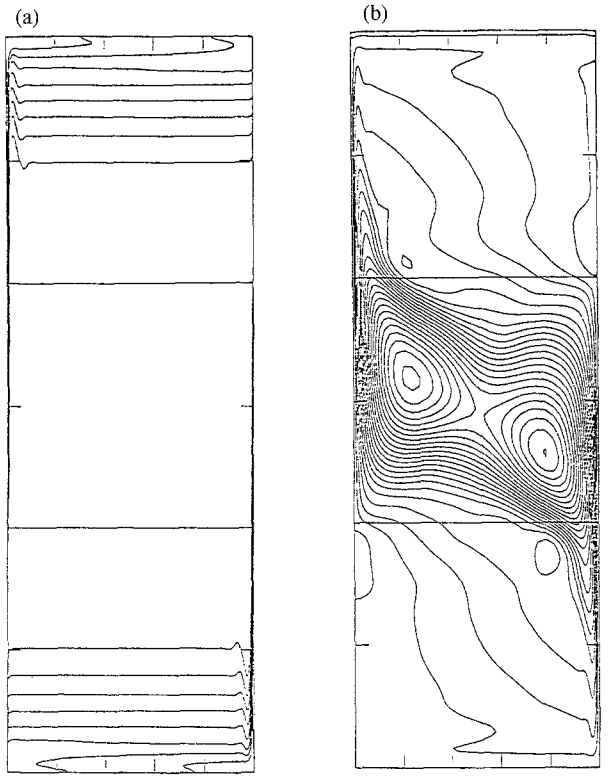

Fig. 5. Computed concentration (a) and velocity (b) fields for $t = 30$ min. $\Delta c = 0.01$ and $\Delta\psi = e^{-3}$.

differences, buoyancy effects will make the lighter fluid reverse its path and turn upward. On their way up to the vertical position where the average concentration equals their own, the fluid elements gain momentum, and at this point the buoyancy force changes direction again. The result is local spacial undulations of the iso-concentration lines, which can be clearly seen close to the lower right corner in Figs 4(a) and 5(a).

In Fig. 4, the flow has begun to attain boundary layer character caused by the relatively weak stratification which is shown by the dashed curve in Fig. 6. The effect of stratification on the velocity field can be investigated using similarity solutions [12] or the exact solution by Gill [8], page 525, which both show that the boundary layer thickness for linear stratification is proportional to the stratification raised to the power 1/4. If the local stratification and the value of $(c'_{\text{wall}} - c'_0)$ at $x = -0.5$ and $t' = 12$ min are taken from the numerical simulation, the solution by Gill, $\delta_S = (4\nu D/\beta g S)^{1/4}$ where S is the stratification, gives a velocity boundary layer thickness that is only $\sim 30\%$ of that shown in Fig. 3. The discrepancy is explained by the decreasing stratification upstream of $x = -0.5$ in Fig. 6, which gives thicker boundary layers which are convected downwards. The reason why Gill's exact solution is considered relevant despite its application to detraining flow, is the weakness of the stratification which causes only a weak horizontal motion. For stronger nonlinear stratification, Gill's solution gives increasingly inaccurate approximations of the actual flow field. Applied to the present case, however, it verifies that even a very weak stratification has a strong effect on the velocity field. In the study by Poujol *et al.* [18], a flow situation similar to the present one is computed, and the decreasing boundary layer thickness is explained by those authors to be caused by interaction with flow reflected by the opposite wall. Due to the very weak interaction between the boundary layers in the present case, and the conclusions drawn here about the strong influence of stratification, the explanation by Poujol *et al.* [18] seems somewhat questionable.

The increased stratification in Fig. 5(a) has reduced the boundary layer thickness further compared to the previous Figures, and in the lower parts of the cell the boundary layer thickness is found to be approximately constant. This is also in accordance with the previously mentioned power law function derived by Gill [8], which for stronger stratification gives a relatively weak relationship between the local stratification and the boundary layer thickness. Even though this function is only valid for linear stratification where the flow is neither detraining nor entraining, the approximately constant vertical boundary layer

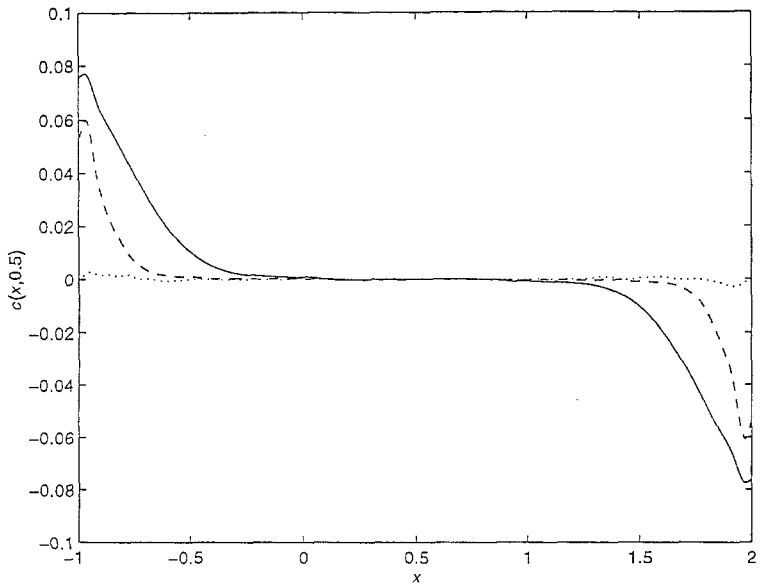

Fig. 6. Stratification along the vertical centerline of the cell. $\Delta c = 0.01$. Duration, t: (——) 30, (– – – –) 12 and (. . . . .) 2 min.

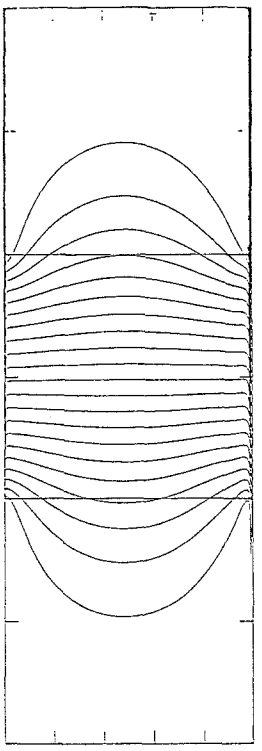

Fig. 7. Streamlines for the electric current in the electrolyte after 30 min. $\Delta i = 5.0$.

thickness in combination with the non-linear stratification in Fig. 5 indicates that a function similar to the power law function above exists also in the present case.

The development of the current density on the electrodes is found to take place in two different stages. The first stage coincides with the development of the diffusion layers when the current is first turned on. Since the current density is dependent on the supply of cupric ions in the electrolyte at the cathode, the initially undisturbed concentration in this area allows a large current density. After about 30 s, the concentration boundary layers are fully developed and the current stabilizes on a level approximately 5% below its initial peak value. The concentration variations across the boundary layers on anode and cathode are then around 20% of the bulk concentration.

Stage two is identified by stable current densities and lasts up to one hour. At this time, stratification in the bulk begins to affect the electrodes. After 30 min the stratification between the electrodes is still very weak, as shown in Fig. 6. The electric potential in the central region is therefore approximately given by the solution to Laplace's equation according to Equation 13, and the current density is easily derived from Equations 2 and 4. Because of the small thickness of the concentration boundary layers along the electrodes and the relatively small concentration changes across them, the current density at the electrode surfaces is approximately equal to the current distribution just outside the boundary layers. Wagner [31] has formulated boundary conditions for this problem, and solved it for the extreme cases of either a very small or a very large distance between the electrodes. For small values of the applied voltage, Wallgren *et al.* [32] have found a solution applicable to the present problem.

Figure 7 shows the current lines after 30 min. They pass partly outside the electrode area which indicates that the effect from variations in bulk resistance will arrive earlier than changes in the concentration over-potential. The current density on the electrodes after 30 min is shown in Fig. 8. The U-shaped form is characteristic for the geometry of the present cell with finite electrodes embedded in plane walls on opposite side. The regions of increased current density at the edges will become smaller as the distance between the electrodes decreases.

3.1. *Comparison between theory and experiments*

Although the numerical simulations were two-dimensional, it was found that viscous effects from the insulated side walls parallel to the x–y-plane considerably influenced the flow field in the experimental cell during the early stages of the electrolysis. Viscous diffusion from these walls damped the velocity field created at the electrodes, thus preventing the central

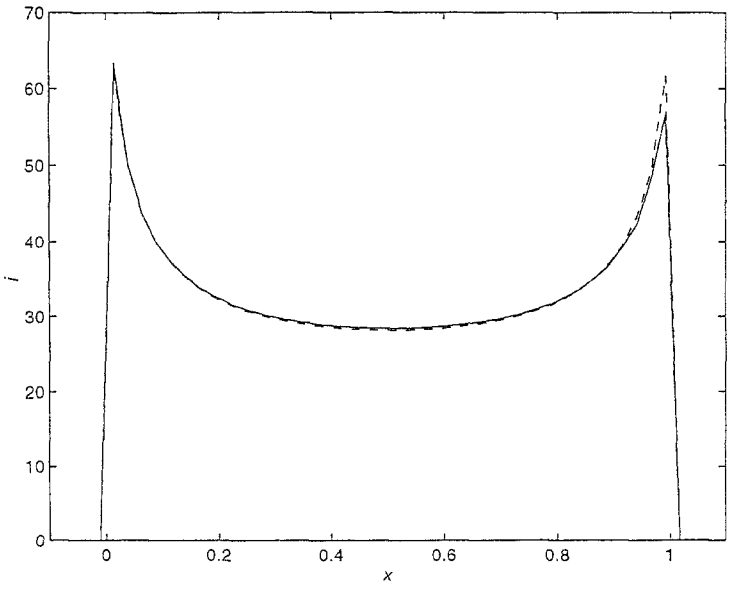

Fig. 8. Current density on electrodes after 30 min. (– – – –) Anode; (——) cathode.

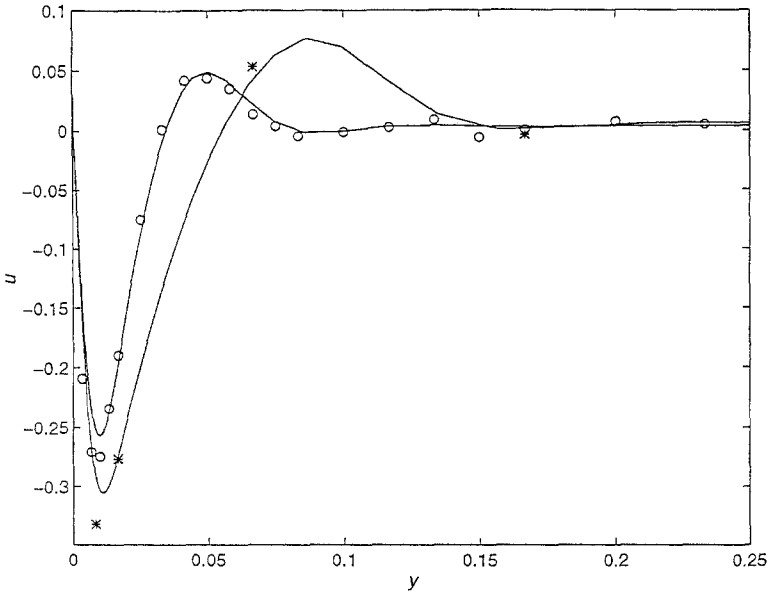

Fig. 9. Comparison between numerically simulated and measured velocity profiles at $x = -0.5$ and $t = 15$ and $t = 30$ min. Key: (——) Numerical solutions; (0——0) experimental data for $t = 30$ min; (∗——∗) experimental data for $t = 15$ min.

vortex found in the fully two dimensional computations to appear in the experiments. As the stratification increased and began to dominate the flow field, the agreement between theory and experiments improved. When the thickness of the velocity boundary layers had decreased to only a few diffusion layer thicknesses, three-dimensional effects in the experimental cell were no longer important. Since the main mechanism for concentration redistribution in the cell is the convective transport in the diffusion boundary layers, and three-dimensional viscous effects in the experimental cell do not significantly influence the velocity field inside these layers, it is believed that the evolution of the concentration field is largely equivalent to that calculated numerically.

Figure 9 shows velocity profiles after 15 and 30 min. The overall agreement between experimental measurements and the numerical computations is good, indicating that the argumentation above about the vanishing influence of the nonelectrode side walls is correct. Only a modest disagreement is found for the peak value of the velocity, where the experimentally measured values are about 10% higher than those computed.

The agreement between numerical results and experimental concentration measurements is also good. The concentration gradient at the surface is equal to the dimensionless current density, and Fig. 10 shows three horizontal concentration profiles at the cathode after 30 min. The increased current density close to the edges of the cathode, which can be seen in Fig. 8, corresponds in Fig. 10 to the increased concentration gradients at the cathode boundary for $x = 0.1$ and $x = 0.9$. Below the cathode, the experimentally measured concentration gradients were somewhat larger than those computed.

3.2. *Exploratory measurements on a larger cell*

Both velocity and concentration measurements were also carried out on a cell where the central part including the electrodes were identical to that in Fig. 1, but where the regions above and below the electrodes were prolonged. This design was made in order to avoid

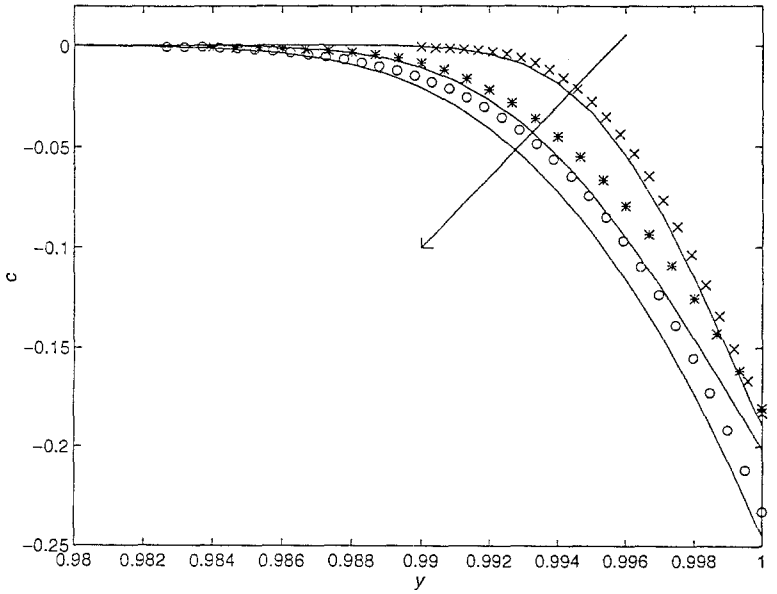

Fig. 10. Comparison between numerically simulated (solid lines) and measured (symbols) concentration profiles at the cathode after $t = 30$ min. $x = 0.1$, 0.5 and 0.9.

stratification between the electrodes for a longer time period, during which it was expected to find a time-independent velocity field. The height of the extended regions was approximately ten electrode lengths each.

The concentration measurements showed that despite the modified geometry, a very weak stratification also started to develop early in this cell. The existence of a stratification was verified by the velocity measurements which registered a decreasing boundary layer thickness, although this decrease was slower than for the smaller cell. A quasisteady velocity field in the electrode area for intermediate times was therefore not found, which is a somewhat unexpected result of the present study, whose explanation is left for future work.

Acknowledgements

This work was partially supported by the Swedish National Board for Industrial and Technical Development. Valuable advice on the choice and implementation of the numerical method was provided by Dr Mårten Levenstam.

References

[1] C. Wagner, *Trans. Electrochem. Soc.* **95** (1949) 161–73.
[2] Y. Awakura, Y. Takenaka and Y. Kondo, *Electrochim. Acta* **21** (1976) 789–97.
[3] Y. Awakura, Y. Maruoka and Y. Kondo, *Denki Kagaku* **4** (1977) 207–12.
[4] F. Fukunaka and Y. Kondo, *Electrochim. Acta* **26** (1981) 1537–46.
[5] F. Fukunaka, T. Minegishi, N. Nishioka and Y. Kondo, *J. Electrochem. Soc.* **128** (1981) 1274–80.
[6] F. Fukunaka and Y. Kondo, *Metall. Rev. MMIJJ* **5** (1988) 10–23.
[7] F. H. Bark and F. Alavyoon, *Appl. Sci. Res.* **53** (1994) 11–34.
[8] A. E. Gill, *J. Fluid Mech.* **26** (1966) 515–36.
[9] S. Kimura and A. Bejan, *ASME J. Heat Transf.* **106** (1984) 98–103.
[10] B. Gebhart, Y. Jaluria, R. L. Mahajan and B. Sammakia, Springer-Verlag, Berlin (1988).
[11] V. I. Semenov, *Heat Transf. Sov. Res.* **16** (1984) 69–85.
[12] R. A. W. M. Henkes and C. J. Hoogendoorn, *Int. J. Heat Mass Transf.* **32** (1989) 147–55.
[13] S. W. Webb, *ASME Heat Transf. Div. (HTD)* **107** (1989) 197–206.
[14] M. G. Worster and A. M. Leitch, *J. Fluid Mech.* **156** (1985) 301–19.
[15] V. P. Carey, *Int. J. Heat Mass Transf.* **26** (1983) 911–18.
[16] *Idem, ibid.* **27** (1984) 419–31.
[17] J. M. Hyun, *Adv. Heat Transf.* **24** (1994) 277–319.
[18] F. Poujol, J. Rojas and E. Ramos, *Int. J. Heat Fluid Flow* **14** (1993) 357–65.
[19] R. I. Karlsson, F. Alavyoon and A. Eklund, 'Laser Anemometry Advances and Applications', BHRA/Springer-Verlag (1990) pp. 329–37.
[20] A. Eklund, F. Alavyoon, D. Simonsson, R. I. Karlsson and F. H. Bark, *Electrochim. Acta* **36** (1991) 1345–54.
[21] F. H. Bark, F. Alavyoon and A. A. Dahlkild, *J. Fluid Mech.* **235** (1992) 665–89.
[22] A. Bejan, 'Convection Heat Transfer', J. Wiley & Sons, New York (1984) p. 114.
[23] J. S. Newman 'Electrochemical Systems', Prentice-Hall, Englewood Cliffs, NJ (1991).
[24] B. Landholt-Börnstein 'Numerical Data and Functional Relationships in Science and Technology', New Series **5**(II)', Springer-Verlag, Berlin (1967).
[25] N. Tanaka and R. Tamamushi *Electrohcim. Acta* **9** (1964) 963.
[26] C. A. J. Fletcher, 'Computational Techniques for Fluid Dynamics', 2nd edn. Springer-Verlag, Berlin (1991).
[27] J. Shen, *Int. J. Numer. Methods Fluids* **16** (1993) 249–53.
[28] R. W. Freund, *SIAM J. Sci. Comput.* **14** (1993) 470–84.
[29] G. H. Golub and C. F. van Loan, 'Matrix Computations', 2nd edn. Johns Hopkins Press Ltd., London (1989).
[30] R. Eriksson, Licentiate thesis, Dept. of Chem. Eng. Tech., Royal Inst. Tech., Stockholm (1995).
[31] C. Wagner, *J. Electrochem. Soc.* **98** (1951) 116–28.
[32] C. F. Wallgren, F. H. Bark and B.-J. Andersson, *Electrochim. Acta* (1996) submitted.